NASA/TM—2010-216363

Two-Speed Gearbox Dynamic Simulation Predictions and Test Validation

David G. Lewicki
Glenn Research Center, Cleveland, Ohio

Hans DeSmidt
University of Tennessee, Knoxville, Tennessee

Edward C. Smith
Penn State University, University Park, Pennsylvania

Steven W. Bauman
Glenn Research Center, Cleveland, Ohio

May 2010

NASA STI Program . . . in Profile

Since its founding, NASA has been dedicated to the advancement of aeronautics and space science. The NASA Scientific and Technical Information (STI) program plays a key part in helping NASA maintain this important role.

The NASA STI Program operates under the auspices of the Agency Chief Information Officer. It collects, organizes, provides for archiving, and disseminates NASA's STI. The NASA STI program provides access to the NASA Aeronautics and Space Database and its public interface, the NASA Technical Reports Server, thus providing one of the largest collections of aeronautical and space science STI in the world. Results are published in both non-NASA channels and by NASA in the NASA STI Report Series, which includes the following report types:

- TECHNICAL PUBLICATION. Reports of completed research or a major significant phase of research that present the results of NASA programs and include extensive data or theoretical analysis. Includes compilations of significant scientific and technical data and information deemed to be of continuing reference value. NASA counterpart of peer-reviewed formal professional papers but has less stringent limitations on manuscript length and extent of graphic presentations.

- TECHNICAL MEMORANDUM. Scientific and technical findings that are preliminary or of specialized interest, e.g., quick release reports, working papers, and bibliographies that contain minimal annotation. Does not contain extensive analysis.

- CONTRACTOR REPORT. Scientific and technical findings by NASA-sponsored contractors and grantees.

- CONFERENCE PUBLICATION. Collected papers from scientific and technical conferences, symposia, seminars, or other meetings sponsored or cosponsored by NASA.

- SPECIAL PUBLICATION. Scientific, technical, or historical information from NASA programs, projects, and missions, often concerned with subjects having substantial public interest.

- TECHNICAL TRANSLATION. English-language translations of foreign scientific and technical material pertinent to NASA's mission.

Specialized services also include creating custom thesauri, building customized databases, organizing and publishing research results.

For more information about the NASA STI program, see the following:

- Access the NASA STI program home page at *http://www.sti.nasa.gov*

- E-mail your question via the Internet to *help@sti.nasa.gov*

- Fax your question to the NASA STI Help Desk at 443–757–5803

- Telephone the NASA STI Help Desk at 443–757–5802

- Write to:
  NASA Center for AeroSpace Information (CASI)
  7115 Standard Drive
  Hanover, MD 21076–1320

NASA/TM—2010-216363

Two-Speed Gearbox Dynamic Simulation Predictions and Test Validation

David G. Lewicki
Glenn Research Center, Cleveland, Ohio

Hans DeSmidt
University of Tennessee, Knoxville, Tennessee

Edward C. Smith
Penn State University, University Park, Pennsylvania

Steven W. Bauman
Glenn Research Center, Cleveland, Ohio

Prepared for the
66th Annual Forum and Technology Display (AHS Forum 66)
sponsored by the American Helicopter Society
Phoenix, Arizona, May 11–13, 2010

National Aeronautics and
Space Administration

Glenn Research Center
Cleveland, Ohio 44135

May 2010

Level of Review: This material has been technically reviewed by technical management.

Available from

NASA Center for Aerospace Information
7115 Standard Drive
Hanover, MD 21076–1320

National Technical Information Service
5301 Shawnee Road
Alexandria, VA 22312

Available electronically at http://gltrs.grc.nasa.gov

Two-Speed Gearbox Dynamic Simulation Predictions and Test Validation

David G. Lewicki
National Aeronautics and Space Administration
Glenn Research Center
Cleveland, Ohio 44135

Hans DeSmidt
University of Tennessee
Knoxville, Tennessee 37996

Edward C. Smith
Penn State University
University Park, Pennsylvania 16802

Steven W. Bauman
National Aeronautics and Space Administration
Glenn Research Center
Cleveland, Ohio 44135

Abstract

Dynamic simulations and experimental validation tests were performed on a two-stage, two-speed gearbox as part of the drive system research activities of the NASA Fundamental Aeronautics Subsonics Rotary Wing Project. The gearbox was driven by two electromagnetic motors and had two electromagnetic, multi-disk clutches to control output speed. A dynamic model of the system was created which included a DC electric motor with proportional-integral-derivative (PID) speed control, a two-speed gearbox with dual electro-magnetically actuated clutches, and an eddy current dynamometer. A six degree-of-freedom model of the gearbox accounted for the system torsional dynamics and included gear, clutch, shaft, and load inertias as well as shaft flexibilities and a dry clutch stick-slip friction model. Experimental validation tests were performed on the gearbox in the NASA Glenn gear noise test facility. Gearbox output speed and torque as well as drive motor speed and current were compared to those from the analytical predictions. The experiments correlate very well with the predictions, thus validating the dynamic simulation methodologies.

Nomenclature

A_p	EMA pole face area
$\mathbf{C}$	damping matrix
e	set-point speed error
f_{ni} [i = 1,2]	EMA clutch actuation force
$f_{ni,\max}$	maximum actuation force
$\mathbf{F}_c$, $\mathbf{F}_{TL}$, $\mathbf{F}_{Tm}$	generalized forces
h_0, h_d	coil static and dynamic air gap
I_c	EMA coil current
$I_{c\max}$, I_{csat}	maximum and saturation coil current
I_m	motor armature current
i	i^{th} clutch or i^{th} gear
J_{cdi}, J_{cfi} [i = 1,2]	clutch disk and clutch flange inertias
J_L, J_m	dynamometer and motor inertias
J_{gi} [i = 1,6]	gear rotational inertias
k_p, k_I, k_d	motor PID speed control gains
k_{mc1}, k_{c1c2}, k_{sl}, k_{c2L}	shaft torsional stiffness's
k_{mb}, k_{mt}	motor back EMF and torque constant
k_s	clutch separator spring constant
$\mathbf{K}$	stiffness matrix
L_m	motor circuit inductance
$\mathbf{M}$	mass matrix
n_{12}, n_{34}, n_{56}	gear ratios
N_d	number of clutch disks
N_w	number EMA coil windings
$\mathbf{q}$	DOF vector
$\mathbf{q}_{II}$, $\mathbf{q}_{III}$, $\mathbf{q}_{IV}$	constrained DOF vectors
Q	total generalized force vector
R_m, R_c	motor and EMA coil electrical resistance
R_d, R_o	clutch disk inner and outer radii
t	time
T	system kinetic energy
T_L, T_m	dynamometer and motor torques
T_{ci} [i = 1,2]	EMA clutch torques
$T_{ci,II}$, $T_{ci,III}$, $T_{ci,IV}$	clutch torques (kinematically locked)
$T_{ci,\max}$ [i = 1,2]	maximum static clutch torques
$T_{ci,slip}$ [i = 1,2]	slipping clutch torques
V	system strain energy
V_{ci} [i = 1,2]	EMA clutch coil voltage
$V_{c\max}$	maximum clutch coil voltage
V_d	dynamometer voltage
V_m	motor armature voltage
Z_i [i = 1,6]	number of gear teeth

δ	Stribeck exponent (empirical)
δW	virtual work
ε	slip-stick threshold tolerance
ϕ_{cdi}, ϕ_{cfi} [i = 1,2]	clutch disk and flange rotation
ϕ_{gi} [i =1–6]	gear rotations
ϕ_L, ϕ_m	load and motor rotation
μ_0	free space permeability (air)
μ_k, μ_s	kinetic and static friction coefficients
μ_{stb}	Dry friction coefficient (Stribeck)
ξ_s	viscous damping parameter
Ω_{cfi}, Ω_{cdi} [i = 1,2]	clutch disk and flange speed
Ω_L, Ω_m	load and motor speed
Ω_{set}	motor set-point speed
Ω_{si} [i = 1,2]	slip speed
Ω_{stb}	Stribeck velocity (empirical)

Introduction

As part of the Subsonic Rotary Wing Project of the NASA Fundamental Aeronautics Program, research is being performed for large civil tiltrotors to replace regional airliners over medium ranges to alleviate next-generation air traffic. The tiltrotor is designed to carry 90 passengers for 1000 nm with performance of 300 knots at 28,000-ft altitude. Aircraft sizing-design studies have identified that a two-speed rotor configuration is required (Refs. 1 and 2). Rotor speed at cruise is required to be reduced, possibly down to 50 percent of hover speed, to keep rotor blade advancing tip speeds reasonable. To support this configuration, research in developing two-speed gearboxes as well as dynamic modeling of multi-speed rotorcraft drive systems is being led at the Glenn Research Center with help from university counterparts.

As a brief background, one early study of a multi-speed rotorcraft drive system consisted of a high-speed traction drive variator and a planetary differential gear unit (Ref. 3). A unit was tested and performed as designed. However, the mechanical efficiency was lower than that of a conventional drive system. Also, the use of traction drives for a main drive path is not an accepted practice for U.S. rotorcraft manufacturers. Previous studies have been sponsored by NASA to investigate multi-speed drive systems (Refs. 4 and 5). These studies looked at earlier tiltrotor applications where 15 percent speed reduction for cruise was required. Dual-path configurations and compound planetary configurations looked promising. However, major concerns that were found included shifting and drive system weight. An electro-mechanical, infinitely-variable transmission, comprising a pair of planetary trains interconnected with two electric machines and clutches, has been proposed (Ref. 6). Again, the mechanical efficiency suffered as well as the added complexity of two planetary systems. Also, a unique concept called a pericyclic continuously variable-speed transmission is being investigated (Ref. 7). It uses pericyclic kinematics to achieve single-speed reduction ratios between 1.05:1 to 50:1 with variable-speed capability in one configuration. This concept, however, has yet to be tested. In summary, the results from the previous studies indicates that the incorporation of multi-speed concepts in rotorcraft application is not a trivial process and adds complexity and weight. Thus, further research and development in this area is required, such as described in (Ref. 8). In addition, dynamic modeling of multi-speed drive systems can help define the characteristics and limitations of the drive systems and the shifting process.

Since very few multi-speed rotorcraft studies have been published, very little work on dynamic modeling for multi-speed rotorcraft drive systems has been done. There has been, however, numerous publications on dynamic modeling of automotive drive systems. Much of the work addresses the automatic transmission shifting control with emphasis on maximizing fuel economy and maintaining performance (Refs. 9 to 15). For these, the typical system being modeled is the gasoline internal combustion engine, torque convertor, multi-speed gearbox, tires and vehicle dynamics, as well as throttle and shifting controls. Dynamic speed, gear ratio, and torque are some of the parameters predicted. This strategy has been applied to hybrid power trains (Refs. 16 and 17), continuously variable transmissions (Refs. 18 to 22), and even heavy trucks and tanks for the military (Refs. 23 to 27). The modeling in the automotive field has had much success in improving drive train development. The approach and some modeling tools can be extended to the rotorcraft arena. However, specifics of integration of the gas turbine engine, multi-speed drive systems, clutches, and the dynamics of the rotor and rotorcraft vehicle have yet to been addressed for rotorcraft application.

A NASA Research Announcement (NRA) contract was awarded to the team of Penn State University, the University of Tennessee, and the University of Michigan, to develop a dynamic model of a multi-speed rotorcraft drive system. The model integrates the dynamics of the gas turbine engine, multi-speed transmission system, and rotor system. System models for conventional helicopters and tiltrotors are being developed.

The objective of the current study is to validate a gearbox dynamic model developed under the NRA award. As a first step in the model validation process, a dynamic model of a two-speed gearbox developed at NASA for lunar space application was derived. This was an existing two-speed gearbox available for test. Experimental tests were performed on the gearbox as installed on a dynamometer. Speeds and torques were measured and compared to predictions during various shifting profiles.

Chariot Gearbox Description

The Glenn Research Center designed and fabricated a gearbox for use on the NASA Chariot vehicle. The Chariot is the next-generation rover vehicle for lunar exploration (Fig. 1) and was designed by the NASA Johnson Space Center (JSC) for truck-type utility operations on the moon. This includes the

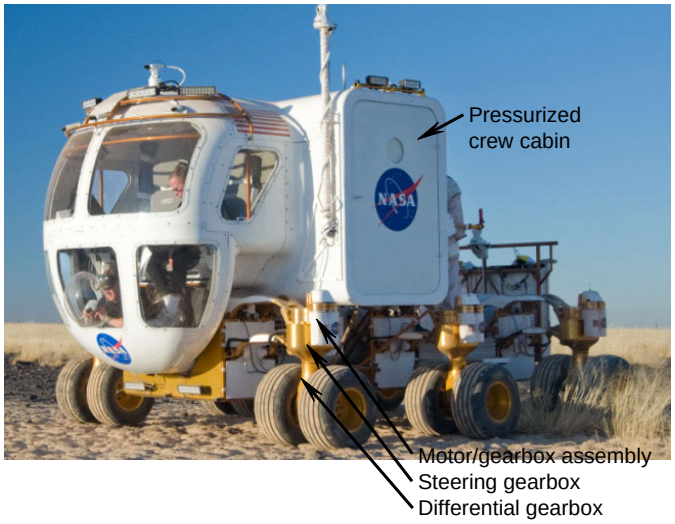

Figure 1.—NASA Chariot lunar rover vehicle.

ability to carry astronauts and substantial amounts of equipment, rocks, or soil. It can be fitted with a soil-moving blade and the flat-top deck of the vehicle lends itself to custom configurations for different missions. It can also be outfitted with a pressurized crew cabin as shown in Figure 1.

The Chariot has six identical and independently-controlled motor-driven wheel pods, three on each side of the vehicle. Each pod has a pair of driven wheels for a total of 12 wheels. Multiple wheels and pods creates redundancy for reliability and reduces the tire surface contact pressure. All six pods and wheel pairs can be steered independently and to any angle (a full 360° capability), making the vehicle highly maneuverable. Each pod has its own combination passive and active suspension. The active part allows for adjusting the chassis height, including lowering it to the ground, which allows for easy egress of the astronauts and easier loading and unloading of cargo.

Each pod is driven by a motor/gearbox assembly. The output passes through a steering gearbox, then to a differential gearbox, and then to each wheel (Fig. 1). The motor/gearbox assembly is the subject of the current study and will be further called the Chariot gearbox for simplicity. The original Chariot gearbox was designed by JSC and is shown in Figure 2. Due to a tight schedule, the JSC Chariot gearbox was designed and fabricated using readily available off-the-shelf commercial gears, bearings, shafts, electric clutches, and electric motors. Two brushless electric servo motors drive the unit, both to generate adequate power and for motor redundancy. The motors are rated for 300 V DC and each one draws up to 8 A to produce 2.8 hp at peak efficiency. The original gearbox design utilizes a total of 12 gears, 17 bearings, and 7 different shafts. It has two selectable speed ratios. The low speed provides a 16:1 gear reduction for a vehicle speed of about 3 mph while the high speed provides a 4:1 gear reduction for a vehicle top speed of 12 mph. The speed selection is accomplished with two electric clutches.

The NASA Glenn Research Center (GRC) used their rotorcraft drive system experience to redesign the Chariot

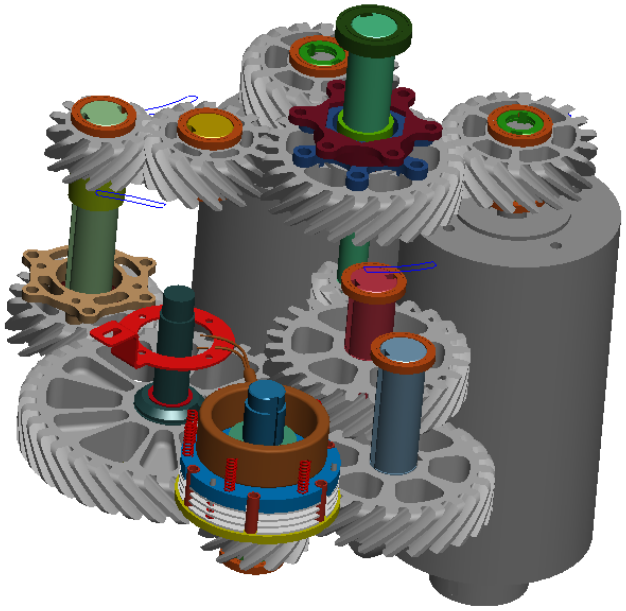

Figure 2.—NASA Johnson Space Center Chariot gearbox design.

gearbox. The gearbox was redesigned as a direct replacement to the JSC design, but used gear design practices of the current rotorcraft industry to reduce the number of components as well as weight and size. To allow direct replacement in the Chariot vehicle, the same servo motors were used in the redesign as well as the same gearbox mounting pattern and output shaft connection. Custom-made high-strength gears allowed the use of lighter and fewer gears (7 instead of 12), and the gear train consists of just two parallel axes, resulting in fewer shafts (3 instead of 7) and fewer bearings (13 instead of 17). A detailed description of the redesign is given in (Ref. 28).

A schematic of the GRC Chariot gearbox is shown in Figure 3. The gearbox is a two-stage, two-speed gearbox. The outputs of the two brushless electric servo motors are attached to pinion gears (Gear 1 in Fig. 3). For the first reduction stage, the pinion gears drive a bull gear (Gear 2) producing a 3.94:1 speed reduction. The bull gear (Gear 2) drives two concentric electromagnetically-actuated (EMA) multi-disk clutches. For low-speed operation, the top clutch (low-speed clutch) is engaged and the bottom clutch (high-speed clutch) is disengaged. The output of the low-speed clutch passes through two sets of spur gears (Gears 3, 4, 5, and 6). This produces a 16.14:1 speed reduction. For high-speed operation, the bottom clutch (high-speed clutch) is engaged and the top clutch (low-speed clutch) is disengaged. The bull gear (Gear 2) output passes directly out the gearbox producing a 3.94:1 speed reduction. Also, Gears 3 to 6 freewheel under no load during high-speed engagement. Design parameters of the gears are given in Table I. The gears were made from AISI 9310 steel and were carburized, hardened, and ground to an AGMA gear tolerance Class 12.

TABLE I.—NASA GLENN RESEARCH CENTER CHARIOT GEARBOX GEAR DESIGN DATA

	Gear 1	Gear 2	Gear 3	Gear 4	Gear 5	Gear 6
No. of teeth	16	63	20	42	21	41
Diametral pitch (teeth/in.)	8	8	10	10	10	10
Circular pitch (in.)	0.393	0.393	0.314	0.314	0.314	0.314
Whole depth (in.)	0.294	0.294	0.235	0.235	0.235	0.235
Addendum (in.)	0.125	0.125	0.100	0.100	0.100	0.100
Chordal tooth thickness (in.)	0.193	0.193	0.156	0.156	0.156	0.156
Pressure angle (deg)	25	25	25	25	25	25
Pitch diameter (in.)	2.000	7.875	2.000	4.200	2.100	4.100
Outside diameter (in.)	2.250	8.125	2.200	4.400	2.300	4.300
Root fillet (in.)	0.050	0.050	0.050	0.050	0.050	0.050
Tip relief (in.)	0.0005	0.0005	0.0005	0.0005	0.0005	0.0005

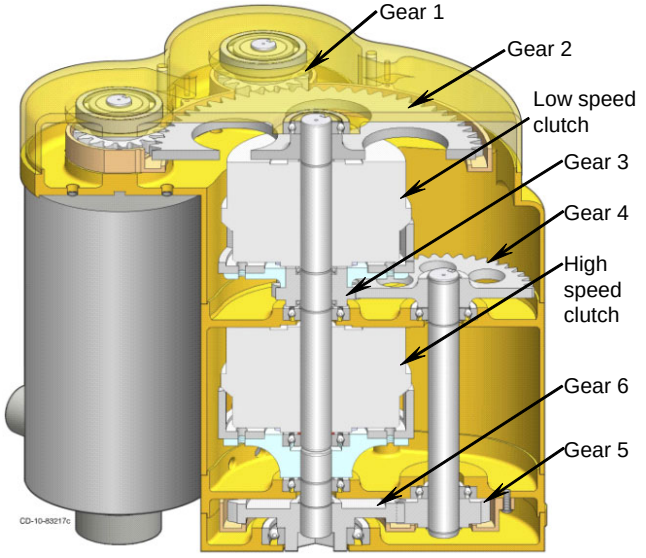

Figure 3.—NASA Glenn Research Center Chariot gearbox design.

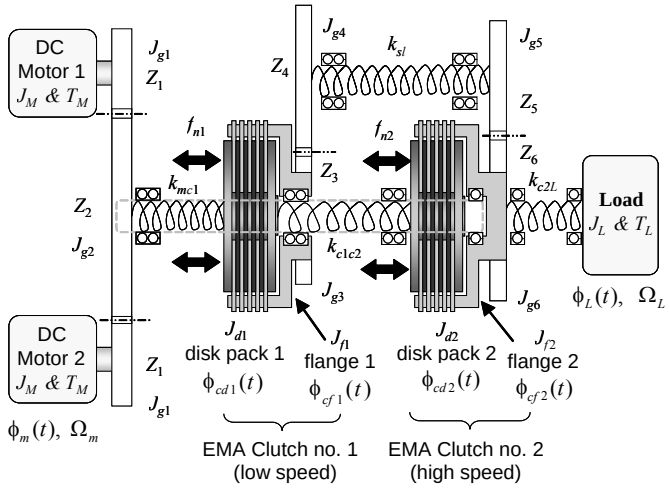

Figure 4.—Dual-clutch gearbox torsional dynamic model.

Commercially available off-the-shelf clutches were used in the redesign due to schedule constraints. Electric multiple disc clutches were used. They provided a maximum torque of 70 lb-ft and were powered by a 24-V DC source, similar to the JSC Chariot application.

The gearbox housing was manufactured from a combination of 6061 and 7075 aluminum alloys. A stacked-component approach was used in the design of the housing. A total of five parts made up the complete housing: 1) upper cover, 2) transition case, 3) deep case, 4) short case, and 5) lower cover. This helped keep the size profile minimized because it allowed the top gear plane, with the two motor pinions and bull gear, to be shrouded closely by way of the top cover before transitioning to the majority smaller profile required for the main body which encompasses the rest of the gears and both electric clutches. The gearbox was grease lubricated, using a grease similar to that used in helicopter tail rotor shaft bearings. Grease-retention shrouds were designed around all gears to hold the applied grease close to the gear teeth.

Chariot Gearbox Modeling

To predict the shift response of the dual-clutch gearbox system, a torsional dynamics model including gear, clutch, shaft and load inertias, as well as shaft torsional flexibilities, and dry clutch stick-slip friction effects was developed. A schematic of the model is shown in Figure 4 and the kinematics is summarized in Equations (1) to (3).

$$\begin{aligned} &\phi_{g1} = \phi_m, \quad \phi_{g2} = -n_{12}\phi_{g1} \\ &\phi_{cf1} = \phi_{g3}, \quad \phi_{g4} = -n_{34}\phi_{g3} \\ &\phi_{g6} = -n_{56}\phi_{g5}, \quad \phi_{cf2} = \phi_{g6} \end{aligned} \tag{1}$$

Here, ϕ_m, is the motor rotation, ϕ_{cd1}, ϕ_{cf1}, are the low-speed clutch (clutch no. 1) disk and flange rotations, ϕ_{cd2}, ϕ_{cf2}, are the high-speed clutch (clutch no. 2) disk and flange rotations, ϕ_{gi} [i =1–6] are the gear rotations, and ϕ_L is the rotation of the

driven load. Also, the gear ratios n_{12}, n_{34} and n_{56} in terms of the number of gear teeth Z_i [i =1–6] are

$$n_{12} = Z_1 / Z_2\,,\ n_{34} = Z_3 / Z_4\,, \text{ and } n_{56} = Z_5 / Z_6 \tag{2}$$

The engagement and disengagement of the EMA clutches is controlled by axial forces, f_{n1} and f_{n2}, applied normal to the clutch disks via electromagnetic actuation forces.

Due to the kinematics, the only condition under which both clutches can be locked simultaneously corresponds to the zero-speed or fully-stalled condition. When both clutches are applied simultaneously the clutches act as a braking system. Thus, during normal operation only one clutch is fully engaged and locked (with full applied engagement force $f_{ni} = f_{ni,\max}$) while the other clutch remains open (with zero applied engagement force, $f_{ni} = 0$). In the low-speed condition clutch no. 1 is locked and clutch no. 2 is open and the transmission output speed, Ω_L, is

$$\text{Low ratio: } \Omega_L = -\frac{Z_1}{Z_2}\frac{Z_3}{Z_4}\frac{Z_5}{Z_6}\Omega_m \tag{3a}$$

and in high-speed condition clutch no. 1 is open and clutch no. 2 is locked

$$\text{High ratio: } \Omega_L = -\frac{Z_1}{Z_2}\Omega_m \tag{3b}$$

where Ω_m is the motor speed.

Based on the unconstrained condition with both clutches slipping, the system kinetic energy can be expressed as

$$\begin{aligned} T = 2\left[\frac{1}{2}(J_m + J_{g1} + {n_{12}}^2 J_{g2})\dot{\phi}_m^2\right] + \frac{J_{cd1}}{2}\dot{\phi}_{cd1}^2 \\ \ldots + \frac{1}{2}(J_{cf1} + J_{g3} + {n_{34}}^2 J_{g4})\dot{\phi}_{cf1}^2 + \frac{J_{cd2}}{2}\dot{\phi}_{cd2}^2 \\ \ldots + \frac{1}{2}(J_{cf2} + J_{g6} + \frac{J_{g5}}{{n_{56}}^2})\dot{\phi}_{cf1}^2 + \frac{J_L}{2}\dot{\phi}_L^2 \end{aligned} \tag{4}$$

where, J_m, J_{cdi}, J_{cfi} [i = 1,2], J_{gi} [i =1–6], and J_L are the rotational inertias of the motor, clutch disks, clutch flanges, gears and load, respectively. Furthermore, the total system strain energy is

$$\begin{aligned} V = \frac{1}{2}\big[k_{mc1}(\phi_{g2} - \phi_{cd1})^2 + k_{c1c2}(\phi_{cd2} - \phi_{cd1})^2 \\ \ldots + k_{c2L}(\phi_L - \phi_{cf2})^2 + k_{s1}(\phi_{g5} - \phi_{g4})^2\big] \end{aligned} \tag{5}$$

where k_{mc1}, k_{c1c2}, k_{sl}, and k_{c2L} are the torsional stiffness values of the motor-clutch 1 shaft, clutch 1-clutch 2 shaft, the low-speed shaft, and outputs shaft, respectively (see Fig 4). Finally the virtual work due to the system torques is

$$\begin{aligned} \delta W = 2T_m\delta\phi_m - T_{c1}\delta(\phi_{cf1} - \phi_{cd1}) \\ \ldots - T_{c2}\delta(\phi_{cf2} - \phi_{cd2}) - T_L\delta\phi_L \end{aligned} \tag{6}$$

where T_m is the applied motor torque, T_{c1} and T_{c2} are the clutch friction torques between the disk and flange, and T_L is the dynamometer load torque on the output shaft.

The equations of motion are obtained using Euler-Lagrange equations

$$\frac{d}{dt}\left[\frac{\partial T}{\partial \dot{\mathbf{q}}}\right] - \frac{\partial T}{\partial \mathbf{q}} + \frac{\partial V}{\partial \mathbf{q}} = Q \tag{7}$$

resulting in

$$\mathbf{M}\ddot{\mathbf{q}} + \mathbf{C}\dot{\mathbf{q}} + \mathbf{K}\mathbf{q} = \mathbf{F}_c(\ddot{\mathbf{q}}, \dot{\mathbf{q}}, f_{n1}, f_{n2}) + \mathbf{F}_{T_L} + \mathbf{F}_{T_M} \tag{8}$$

with generalized coordinate vector

$$\mathbf{q} = [\phi_m \quad \phi_{cd1} \quad \phi_{cf1} \quad \phi_{cd2} \quad \phi_{cf2} \quad \phi_L]^T \tag{9}$$

and with mass and stiffness matrices, **M** and **K**, defined as

$$\mathbf{M} = \begin{bmatrix} 2(J_m + J_{g1} + {n_{12}}^2 J_{g2}) & 0 & 0 & 0 & 0 & 0 \\ 0 & J_{cd1} & 0 & 0 & 0 & 0 \\ 0 & 0 & J_{cf1} + J_{g3} + {n_{34}}^2 J_{g4} & \ldots & 0 & 0 \\ 0 & 0 & \ldots & J_{cd2} & 0 & 0 \\ 0 & 0 & 0 & 0 & J_{cf2} + J_{g6} + \frac{J_{g5}}{{n_{56}}^2} & 0 \\ 0 & 0 & 0 & 0 & 0 & J_L \end{bmatrix} \tag{10a}$$

$$\mathbf{K} = \begin{bmatrix} k_{mc1}{n_{12}}^2 & k_{mc1}n_{12} & 0 & 0 & 0 & 0 \\ k_{mc1}n_{12} & k_{mc1} + k_{c1c2} & 0 & -k_{c1c2} & 0 & 0 \\ 0 & 0 & k_{sl}{n_{34}}^2 & 0 & -k_{sl}\frac{n_{34}}{n_{56}} & 0 \\ 0 & -k_{c1c2} & 0 & k_{c1c2} & 0 & 0 \\ 0 & 0 & -k_{sl}\frac{n_{34}}{n_{56}} & 0 & k_{c2L} + \frac{k_{sl}}{{n_{56}}^2} & -k_{c2L} \\ 0 & 0 & 0 & 0 & -k_{c2L} & k_{c2L} \end{bmatrix} \tag{10b}$$

together with an assumed proportional damping matrix

$$\mathbf{C} = \xi_s\,\mathbf{K} \tag{10c}$$

based on a structural viscous damping factor, ξ_s = 0.00001 (constant). Finally, the generalized force vectors obtained from the virtual work are

$$\delta W = Q^T \delta q \ , \ Q = F_{Tm} + F_c + F_{TL} \tag{11a}$$

with

$$\mathbf{F}_{Tm} = \begin{bmatrix} 2T_m \\ 0 \\ 0 \\ 0 \\ 0 \\ 0 \end{bmatrix}, \ \mathbf{F}_c = \begin{bmatrix} 0 \\ T_{c1} \\ -T_{c1} \\ T_{c2} \\ -T_{c2} \\ 0 \end{bmatrix}, \text{ and } \mathbf{F}_{TL} = \begin{bmatrix} 0 \\ 0 \\ 0 \\ 0 \\ 0 \\ -T_L \end{bmatrix} \tag{11b}$$

where $\mathbf{F}_{Tm}$, $\mathbf{F}_{TL}$, and $\mathbf{F}_c$ are generalized forces due to T_m, T_L, and clutch friction torques T_{c1} and T_{c2}.

The DC electric motor torque, T_m, is computed based on the armature current, I_m, and applied motor control voltage, V_m, as

$$\begin{aligned} L_m \frac{dI_m}{dt} + R_m I_m + k_{mb}\Omega_m &= V_m \\ T_m &= k_{mt} I_m \end{aligned} \tag{12a}$$

where L_m, R_m, k_{mb}, k_{mt} are the motor circuit inductance, resistance, back EMF constant, and torque constant, respectively. Furthermore, V_m is determined using a Proportional Integral Derivative (PID) speed controller

$$V_m = k_p e + k_d \dot{e} + k_I \int e \, dt \tag{12b}$$

which regulates Ω_m to the set point speed Ω_{set} based on the set-point speed error $e = \Omega_{set} - \Omega_m$ and the control gains k_p, k_d, and k_i.

As described in the experimental test setup (see next section), the output shaft of the gearbox is connected to an eddy current dynamometer. In the test runs, the dynamometer is set to operate in so-called constant torque mode. Thus, in the analysis model, the resistive load torque, T_L, is modeled as

$$T_L = T_{L,set} \tanh(V_d \Omega_L) \tag{13}$$

where $T_{L,set}$ is the dynamometer load torque setting and V_d is a scaling voltage. Here, T_L, is essentially a constant resistive torque which approaches zero for small operating speeds.

The clutch torques T_{c1} and T_{c2} are computed based on the instantaneous condition of sticking or slipping as determined from the relative slip velocities between the clutch flanges and disks, $\Omega_{si} = \Omega_{cfi} - \Omega_{cdi}$ [i=1, 2], the axial engagement forces, f_{n1} and f_{n2}, and the clutch dry friction coefficient μ_{stb}. In the case of slipping, T_{ci}, is computed as

$$T_{ci,slip} = \mu_{stb} f_{ni} N_d \frac{4(R_o^3 - R_d^3)}{3(R_o^2 - R_d^2)} \text{sgn}(\Omega_{cfi} - \Omega_{cdi}) \tag{14}$$

where, N_d is the number of friction disks in each clutch pack, and R_d and R_o are the clutch disk inner and outer radii, respectively. Furthermore, μ_{stb} is computed using the so-called Stribeck dry friction model (Ref. 29).

$$\mu_{stb} = \mu_k + (\mu_s - \mu_k) e^{-(|\Omega_{si}|/\Omega_{stb})^\delta} \tag{15}$$

where μ_k is the Coulomb sliding friction coefficient, μ_s is the maximum static friction coefficient, and δ and Ω_{stb} are empirical parameters.

To compute the electromagnetic engagement forces, f_{n1} and f_{n2}, an electro-mechanical model of the EMA clutch is utilized (Eq. (16) and Fig. 5). When a command voltage, V_c, is applied to an EMA clutch coil, magnetic flux is generated which travels axially through the clutch disk pack, across the nominal static air gap, h_0, and the dynamic air gaps, h_d, and then returns via the end plate. Since the coil circuit inductance is a function of the air gaps, the EMA coil current, I_c, is computed from

$$\frac{\mu_0 A_p N_w^2}{2(h_0 + N_d h_d)} \frac{dI_c}{dt} + R_c I_c = V_c(t) \tag{16a}$$

where N_w is the number of coil windings, A_p is the pole face area, μ_0 is the free space permeability of air, and R_c is the coil electrical resistance. Finally, the clutch engagement forces are

$$f_{ni} = \frac{\mu_0 A_p N_w^2 I_c^2}{4(h_0 + N_d h_d)^2} - k_s h_d \ \ [i = 1,2] \tag{16b}$$

where k_s is the clutch disk separator spring stiffness. Furthermore, based on the magnetic saturation limit of the coils, the maximum EMA actuation force is with the clutch full engaged (i.e., with $h_d = 0$)

$$f_{ni\max} = \frac{\mu_0 A_p N_w^2 I_{c\max}^2}{4h_0^2} \ \ [i = 1,2] \tag{17a}$$

and the corresponding static breakaway clutch torque is

$$T_{ci,\max} = \mu_s f_{ni\max} N_d \frac{4(R_o^3 - R_d^3)}{3(R_o^2 - R_d^2)} \ \ [i = 1,2] \tag{17b}$$

With maximum current in the engaged condition

$$I_{c\max} = \frac{1}{R_c} V_{c\max} \le I_{sat} \tag{18}$$

where $V_{c\ \max}$ is maximum applied EMA actuation voltage and I_{sat} is the coil saturation limit.

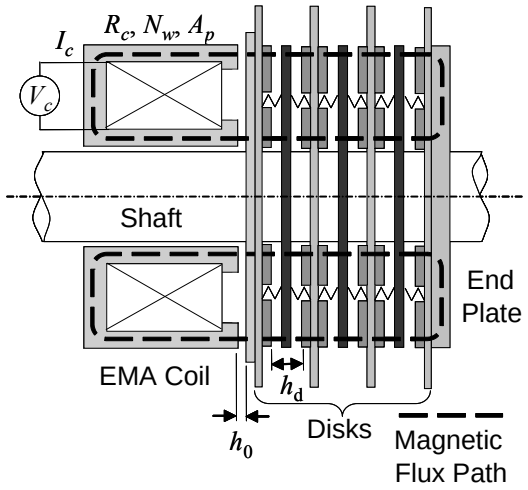

Figure 5.—Electromagnetically actuated (EMA) clutch.

To account for clutch stick-slip and clutch lock-up, four possible system states must be computed and checked at each model simulation time-step. Here, the four possible states are:

I) Both clutches slipping (unconstrained)

$$\begin{aligned} &\text{if} \quad |\Omega_{cf1} - \Omega_{cd1}| > \varepsilon \quad \& \quad |\Omega_{cf2} - \Omega_{cd2}| > \varepsilon \\ &\text{then} \quad T_{c1} = T_{c1,slip}, \quad T_{c2} = T_{c2,slip} \\ &\mathbf{q}_I = \mathbf{q} = [\phi_m \quad \phi_{cd1} \quad \phi_{cf1} \quad \phi_{cd2} \quad \phi_{cf2} \quad \phi_L]^T \end{aligned} \tag{19a}$$

II) Clutch 1 locked - Clutch 2 slipping

$$\begin{aligned} &\text{if} \quad |\Omega_{cf1} - \Omega_{cd1}| \le \varepsilon \quad \& \quad T_{c1,II} \le T_{c1,\max} \\ &\text{then} \quad T_{c1} = T_{c1,II}, \quad T_{c2} = T_{c2,slip} \\ &\mathbf{q}_{II} = [\phi_m \quad \phi_{cd1} \quad \phi_{cd2} \quad \phi_{cf2} \quad \phi_L]^T \end{aligned} \tag{19b}$$

III) Clutch 1 slipping - Clutch 2 locked

$$\begin{aligned} &\text{if} \quad |\Omega_{cf2} - \Omega_{cd2}| \le \varepsilon \quad \& \quad T_{c2,III} \le T_{c2,\max} \\ &\text{then} \quad T_{c1} = T_{c1,slip}, \quad T_{c2} = T_{c2,III} \\ &\mathbf{q}_{III} = [\phi_m \quad \phi_{cf1} \quad \phi_{cd1} \quad \phi_{cd2} \quad \phi_L]^T \end{aligned} \tag{19c}$$

IV) Fully locked (stalled)

$$\begin{aligned} &\text{else} \quad T_{c1} = T_{c1,IV}, \quad T_{c2} = T_{c2,IV} \\ &\mathbf{q}_{IV} = [\phi_m \quad \phi_{cd1} \quad \phi_{cd2} \quad \phi_L]^T \end{aligned} \tag{19d}$$

where ε is a small tolerance below which the slip speed is considered zero and the transmitted clutch torques $T_{c1,II}$, $T_{c2,III}$, $T_{c1,IV}$, and $T_{c2,IV}$ are computed from a kinematic constrained model with corresponding degree-of-freedom vector $\mathbf{q}_{II}$, $\mathbf{q}_{III}$, and $\mathbf{q}_{IV}$ for each locked condition.

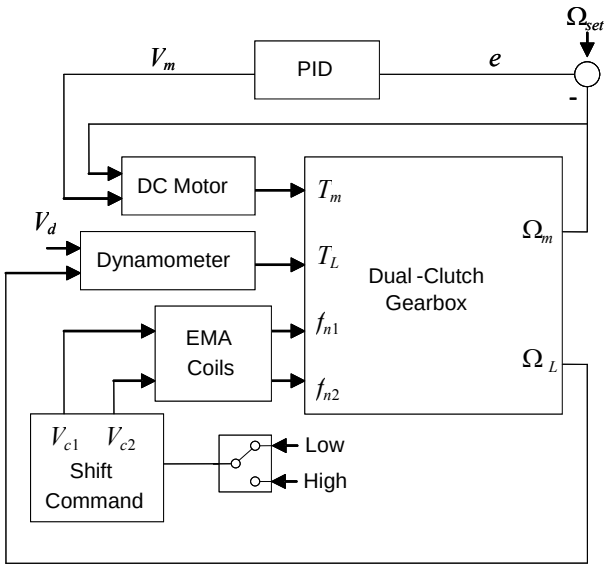

Figure 6.—Dual EMA Clutch/Gearbox system model.

A schematic of the overall system analytical model based on Equations (8) to (19) is given in Figure 6.

To compute the system response, the model is implemented using the Matlab/Simulink (The MathWorks, Inc.) environment where each sub-system (motor, EMA clutch coil, dual gearbox/shaft) are linked via their appropriate physical inputs and outputs. The model parameters used in the experimental validation tests are summarized in Tables II to IV.

TABLE II.—DC MOTOR PARAMETERS

Parameter	Value
Rotational inertia, J_m	0.102 oz-in-sec^2
Motor circuit resistance, R_m	4.0 Ohms
Armature inductance, L_m	13.27×1e-3 H
Back EMF constant, k_{mb}	1.1745 V/sec
Torque constant, k_{mt}	1.1745 Nm/A
Proportional gain, k_p	0.01 V-s
Integral gain, k_I	0.1 V
Derivative gain, k_d	0.001 V-s^2
Set point speed, Ω_{set}	800 rpm

TABLE III.—DYNAMOMETER LOAD PARAMETERS

Parameter	Value
Rotational inertia, J_L	96.06 oz-in-sec^2
Load torque setting, $T_{L,set}$	360 lb-in.
Output shaft stiffness, k_{c2L}	11509 N-m

TABLE IV.—EMA CLUTCH PARAMETERS

Parameter	Value
Outer radius, R_o	2.3125 in.
Inner radius, R_d	0.5625 in.
Number of disks, N_d	4
Free space permeability, μ_0	$4\pi\times10-7$ N·A−2.
Pole face area, A_p	4.43 in.^{2}
Number of coil windings, N_w	600
Nominal Air gap, h_0	0.005 in.
EMA coil resistance, R_c	14 Ohms
Maximum coil voltage, V_{cmax}	24 V
Static friction coefficient, μ_s	0.12
Kinetic friction coefficient, μ_k	0.062*
Stribeck velocity, Ω_{stb}	0.001
Stribeck exponent, δ	1.0
Max static torque, $T_{ci,max}$	70 lb-ft**
Max slipping torque, max($T_{ci,slip}$)	35 lb-ft**

*@ 1800 rpm
** with V_c = 24 V

Apparatus

Experimental validation tests were performed on the Chariot gearbox in the NASA Glenn gear noise test facility. A photograph of the test setup is shown in Figure 7. The Chariot gearbox was mounted on a custom built support table. The gearbox was attached to the support table through the same output mounting as used in the Chariot vehicle. Note that the gearbox was run horizontal in the test setup as compared to vertical in the Chariot vehicle. The output of the Chariot gearbox was connected to a commercially available torquemeter which measured gearbox output torque and speed. The output of the torquemeter was attached to the facility dynamometer which produced a resistance torque on the gearbox. The facility dynamometer was a water-cooled eddy current dynamic absorbing dynamometer with matching controller.

A schematic of the instrumentation and control setup for the experiments is shown in Figure 8. The Chariot gearbox drive motor speed was controlled by a commercially available digital servo motor controller. Drive motor speed was manually adjusted by the operator to a preset value. Gearbox output torque was adjusted by the operator to a preset value using the facility dynamometer and controller. Low-speed and high-speed clutch engagement profiles were pre-programmed using a computer and an analog output card. Voltages from the analog output card for the low and high-speed clutches were routed to individual DC power amplifiers and then to the low- and high-speed clutches, respectively, thus allowing unlimited shifting potential. For each test, the transient Chariot gearbox output speed and torque, as well as the transient drive motor speed and current, were monitored using a facility data acquisition system.

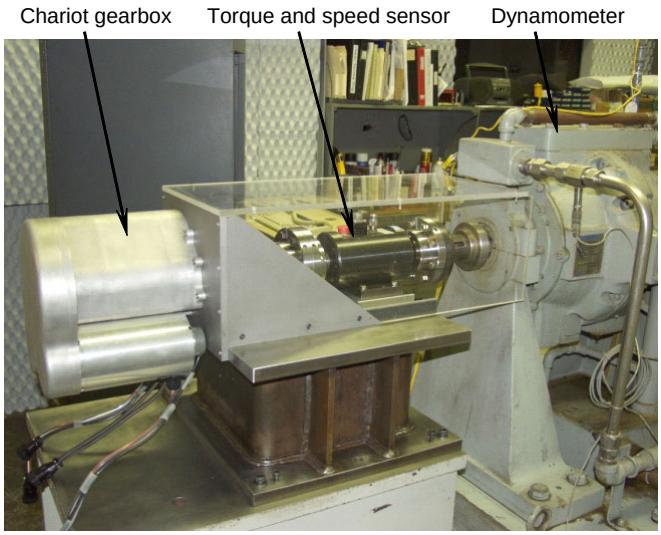

Figure 7.—Chariot gearbox test setup.

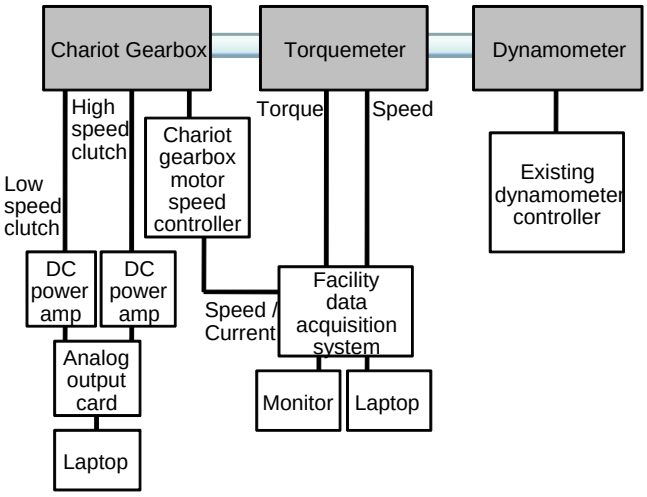

Figure 8.—Chariot gearbox instrumentation and control setup.

Results and Discussion

Two test results are presented. The first is a 1-sec low-to-high speed shifting profile (upshift). The second is a 1-sec high-to-low speed shifting profile (downshift). For the upshift test, the low-speed clutch was engaged at the start of the test. The Chariot gearbox motor speed was set at 800 rpm, which produced a gearbox output speed of 50 rpm. The facility dynamometer was set at 400 lb-in., which produced a gearbox output torque of about 360 to 370 lb-in. as measured by the torquemeter.

For the upshift case, the programmed 1-sec upshift profile was sent to the EMA clutches (Figs. 9(a) and (b)). Here, the low-speed clutch started fully engaged (24-V DC) and linearly decreased to fully disengaged (0-V DC) in 1 sec, while the

high-speed clutch started fully disengaged (0-V DC) and linearly increased to fully-engaged (24-V DC) in 1 sec. The start of the low-speed clutch disengagement occurred at the same time as the start of the high-speed clutch engagement. To simulate the upshift response, the same upshift command voltages (Figs. 9(a) and (b)) were sent to the EMA clutches in the analytical model during the simulation.

The results of the upshift test are given in Figure 9. The start of the shifting occurred at 3 sec in the figure and completed at 4 sec. The Chariot gearbox output speed started to respond to the shift change at about 3.8 sec (Fig. 9(c)). A slight overshot occurred and the output speed settled to a steady value at about 5.5 sec. It should be noted that the overshot could have probably been avoided if further fine tuning of the motor controller would have been performed. However, that was not the objective of the test. The gearbox output torque exhibited a corresponding oscillation during the shifting process (Fig. 9(d)). This was probably due to the speed regime, where the output speed was at the low end of the dynamometer control range. The Chariot gearbox motor itself started to respond to the shift at around 3.4 sec as indicated by an increase in motor current (Fig. 9(g)). There was a slight drop of motor speed at the start of the output speed change, then a corresponding overshot as previously described (Fig. 9(h)).

During test, the drive motor speed and drive motor current were measured from analog outputs of the motor digital servo controller. As a limitation of the controller software, speed and current could only be measured one at a time. Thus, the results from Figure 9 were actually from two separate runs. Identical initial conditions (motor speed and dynamometer torque) and identical shifting profiles were used for the two runs. When compared, the resultant transient Chariot gearbox output speeds (Fig. 9(c)) and torques (Fig. 9(d)) for these two runs were identical, thus validating the repeatability of the experiment.

The corresponding simulation results for the upshift test are also given in Figure 9. The Chariot gearbox output speed simulation also predicted an overshot as with the experiments, with similar results in magnitude but slight phasing differences (Fig. 9(e)). The predicted gearbox output torque (Fig. 9(f)) and predicted drive motor current (Fig. 9(i)) also had oscillations during the shift similar to that from the experiments with similar magnitudes but slight phasing differences. The predicted drive motor speed did not have the initial drop in speed at the start of the shift as with the experiments, but it did have a similar oscillation correction after the shift (Fig. 9(j)). Overall, the predicted results matched quite well to the experiments, especially in magnitude of speed, torque, and current. It should be noted that the exact drive motor controller-speed control parameters were proprietary with the manufacturer. Thus, relative PID gain values could be derived from the control software but exact values used in the simulation had to be assumed. The control parameters of the drive motor had a major impact on the results, and thus could have lead to the discrepancies.

For the downshift test, the high-speed clutch was engaged at the start of the test. The Chariot gearbox motor speed was set at 800 rpm, which produced a gearbox output speed of 200 rpm. The facility dynamometer was set at 400 lb-in., which produced a measured gearbox output torque of about 360 to 370 lb-in. The programmed 1-sec downshift profile was then sent to the EMA clutches (Figs. 10(a) and (b)). For this profile, the low-speed clutch started fully disengaged (0-V DC) and linearly increased to fully engaged (24-V DC) in 1 sec. The high-speed clutch started fully engaged (24-V DC) and linearly decreased to fully disengaged (0-V DC) in 1 sec. The start of disengagement for the high-speed clutch occurred at the same point in time as the start of engagement for the low-speed clutch. To simulate the downshift response, the downshift command voltages (Figs. 10(a) and (b)) were sent to the EMA clutches in the analytical model during the simulation.

The results of the downshift test are given in Figure 10. As with the upshift tests, the start of the shifting occurred at 3 sec in the figure and completed at 4 sec. The Chariot gearbox output speed started to respond to the shift change at about 3.3 sec (Fig. 10(c)). A very slight undershot occurred and the output speed quickly settled to a steady value at about 3.8 sec. The gearbox output torque had a significant drop during the shifting process, with the torque even changing directions (positive to negative in Fig. 10(d)). This was probably due to the dynamometer control during the speed decrease. The Chariot gearbox motor itself started to respond to the shift at about the same time as the gearbox output speed decrease (3.3 sec) as indicated by a slight increase in motor current (Fig. 10(g)). After that, there was a significant momentary decrease in motor current (down to zero) then an increase with an oscillation, then back to a steady-state value. There was a slight increase of motor speed at the start of the output speed change, then a corresponding overshot and return to a steady-state value (Fig. 10(h)).

The corresponding simulation results for the downshift test are also given in Figure 10. The Chariot gearbox output speed simulation also predicted a rather quick drop in speed to the low-speed steady-state value with a very small oscillation (Fig. 10(e)). The predicted gearbox output torque (Fig. 10(f)) also had a significant drop during the shifting process and changed direction as in the experiments. The predicted torque exhibited oscillations during the torque drop. The predicted motor current also showed an increase, sharp decrease to zero, then increase to the steady-state value (Fig. 10(i)). The initial and final steady-state motor currents of the predictions were slightly lower than the measured results. Finally, the predicted drive motor speed had a very similar oscillation during shift as that for the experiments (Fig. 10(j)). Again, the predicted results matched quite well to the experiments, in magnitude and even phase, for speed, torque, and current.

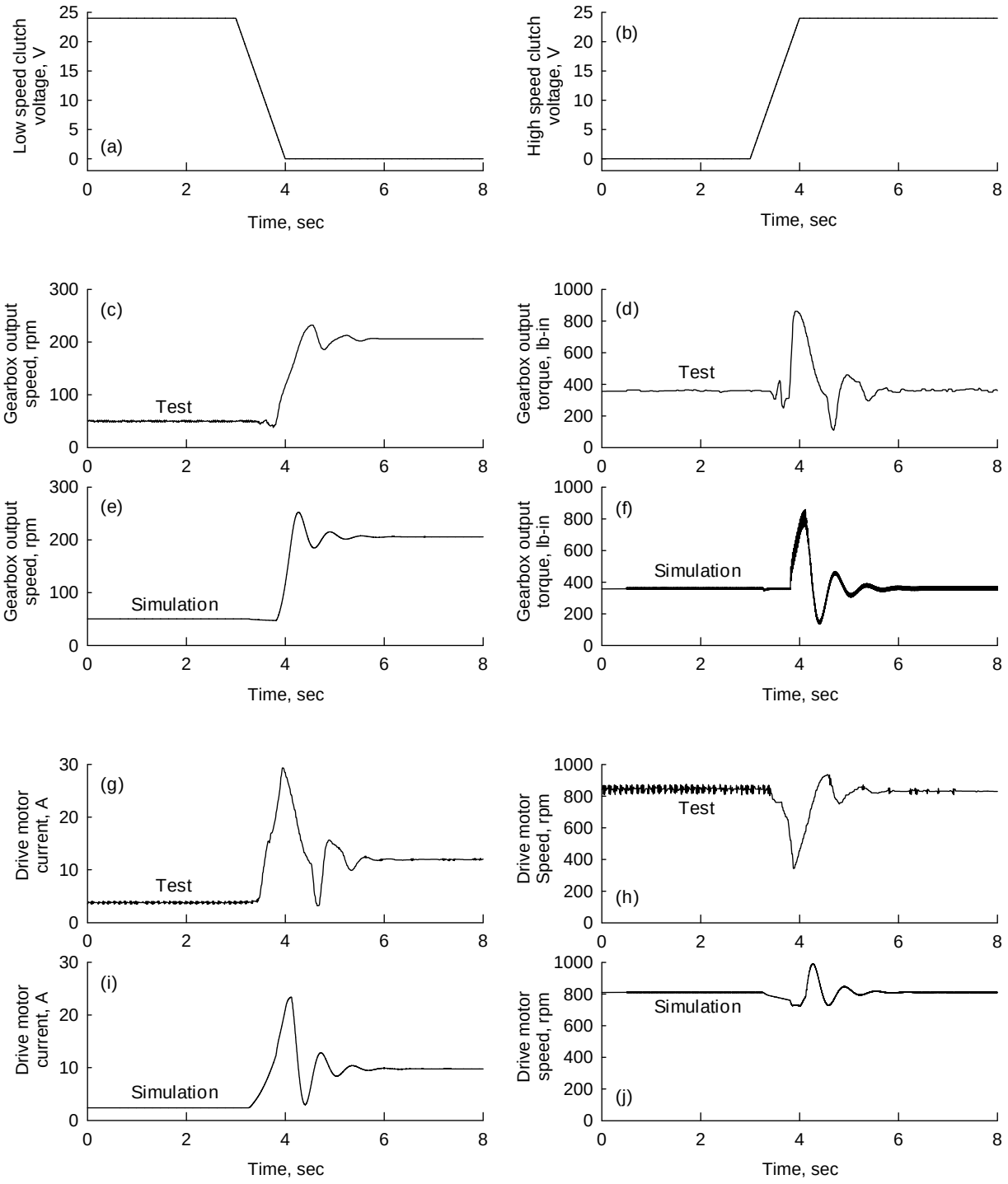

Figure 9.—Comparison of predicted and measured transients for a 1-sec upshift profile.

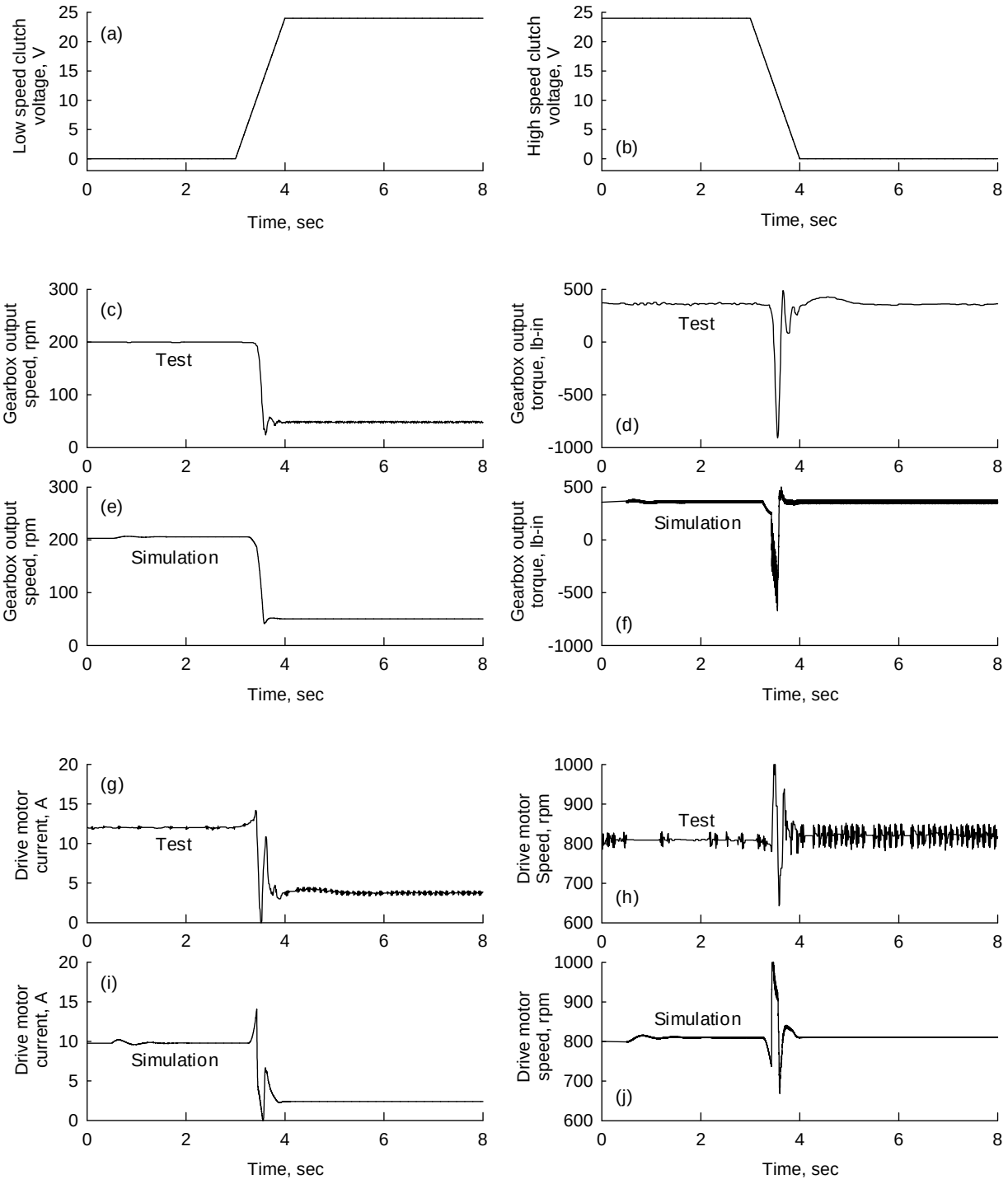

Figure 10.—Comparison of predicted and measured transients for a 1-sec downshift profile.

Conclusions

Dynamic simulations and experimental validation tests were performed on a two-stage, two-speed gearbox as part of the drive system research activities of the NASA Fundamental Aeronautics Subsonics Rotary Wing Project. A dynamic model of the system was created which included a DC electric motor with proportional-integral-derivative (PID) speed control, a two-speed gearbox with dual electro-magnetically-actuated clutches, and an eddy current dynamometer. A six degree-of-freedom model of the gearbox accounted for the system torsional dynamics and included gear, clutch, shaft, and load inertias as well as shaft flexibilities and a dry clutch stick-slip friction model. The simulation was used to predict gearbox performance during shifting scenarios. Experimental validation tests were performed on the gearbox in the NASA Glenn gear noise test facility. Gearbox output speed and torque as well as drive motor speed and current were compared to those from the analytical predictions. The following conclusions were obtained:

1) Overall, the predicted transient results matched quite well to the experiments, especially in magnitude of speed, torque, and current.

2) The control parameters of the drive motor had a major impact on the results, and thus, could have lead to the discrepancies since exact PID values used in the simulation had to be assumed.

3) The transient Chariot gearbox output speeds and torques from the experiments were extremely repeatability.

References

1. Johnson, W., Yamauchi, G.K., and Watts, M.E., "NASA Heavy Lift Rotorcraft Systems Investigation," NASA/TP—2005-213467, Dec. 2005.
2. Acree, C.W., Yeo, H., and Sinsay, J.D., "Performance Optimization of the NASA Large Civil Tiltrotor," International Powered Lift Conference, London, UK, Jul. 22–24, 2008.
3. Goi, T., Kawakami, K., Yamakawa, E., and Tanaka, H., "Variable Rotor Speed Transmission with High Speed Traction Drive," American Helicopter Society 55th Annual Forum, Montreal, Quebec, Canada, May 25–27, 1999.
4. Kish, J., "Vertical Lift Drive System Concept Studies Variable Speed/Two-Speed Transmissions," NASA Contractor Report NASA/CR—2002-211564, Army Research Laboratory Contractor Report ARL–CR–0495, Grant NAG3–2570, Jun. 2002.
5. Bossler, R.B., "Vertical Lift Drive System Concept Studies," NASA Contractor Report NASA/CR—2002-211563, Army Research Laboratory Contractor Report ARL–CR–0496, Grant NAG3–2570, Jun. 2002.
6. Ai, X., Mohr, T., and Anderson, S., "An Electro-Mechanical Infinitely Variable Speed Transmission," SAE 2004 World Congress, Detroit, MI, Mar. 8–11, 2004.
7. Saribay, Z., Smith, E., Lemanski, A., Bill, R., Wang, K.W., and Rao, S., "Compact Pericyclic Continuously Variable Speed Transmission Systems: Design Features and High-Reduction Variable Speed Case Studies," American Helicopter Society 63nd Annual Forum, Virginia Beach, VA, May 1–3, 2007.
8. Stevens, M.A., Handschuh, R.F., and Lewicki, D.G., "Variable/Multispeed Rotorcraft Drive System Concepts," NASA/TM—2009-215456, Army Research Laboratory Report ARL–TR–4758, Mar. 2009.
9. Hong, K., Yang, K., and Lee, K., "An Object-Oriented Modular Simulation Model for Integrated Gasoline Engine and Automatic Transmission Control," SAE transactions, Vol. 108, No. 6, Part 1, pp. 1349–1357, 1999.
10. Haj-Fraj, A., and Pfeiffer, F., "Optimization of Gear Shift Operations in Automatic Transmissions," Proceedings of the 6th International Workshop on Advanced Motion Control, Nagoya, Japan, pp. 469–473, 2000.
11. Jung, G., Cho, B., and Lee, K., "Dynamic Analysis and Closed-Loop Shifting Control of EF-Automatic Transmission with Proportional Control Solenoid Valves," FISITA World Automotive Congress, Seoul, Korea, pp. 12–15, 2000.
12. Gong, J., Zhao, D., Chen, Y., and Chen, N., "Study on Shift Schedule Saving Energy of Automatic Transmission of Ground Vehicles," Journal of Zhejiang University-Science A, Vol. 5, No. 7, pp. 878–883, 2004.
13. Watechagit, S., "Modeling and Estimation for Stepped Automatic Transmission with Clutch-to-Clutch Shift Technology," PhD Dissertation, The Ohio State University, Department of Mechanical Engineering, 2004.
14. Kim, D., Peng, H., Bai, S., and Maguire, J., "Control of Integrated Powertrain with Electronic Throttle and Automatic Transmission," IEEE Transactions on Control Systems Technology, Vol. 15, No. 3, pp. 474, 2007.
15. Lu, X., Xu, X., and Liu, Y., "Simulation of Gear-Shift Algorithm for Automatic Transmission Based on MATLAB," Proceedings of the 2009 World Research Institute World Congress on Software Engineering, pp. 476–480, May 19–21, 2009.
16. Lin, C., Peng, H., Grizzle, J., and Kang, J., "Power Management Strategy for a Parallel Hybrid Electric Truck," IEEE Transactions on Control Systems Technology, Vol. 11, No. 6, pp. 839–849, 2003.
17. Yamamoto, M., Wakahara, T., Okahara, H., and Oshita, H., "Hydraulic System, Shift and Lock-Up Clutch Controls Developed for a Large Torque Capacity CVT," International Continuously Variable and Hybrid Transmission Congress, Paper No. 04CVT–07, 2004.
18. Lu, Z, "Acceleration Simulation of a Vehicle with a Continuously Variable Power Split Transmission," Master's Thesis, West Virginia University, Department of Mechanical Engineering, 1998.
19. Wicke, V., Brace, C., and Vaughan, N., "The Potential for Simulation of Driveability of CVT Vehicles," SAE Transactions, Vol. 109, No. 6, pp. 1205–1210, 2000.
20. Yamamoto, M., Wakahara, T., Okahara, H., and Oshita, H., "Hydraulic System, Shift and Lock-Up Clutch Controls Developed for a Large Torque Capacity CVT," 2004 International Continuously Variable and Hybrid Transmission Congress, Paper No. 04CVT–07, 2004.
21. Klaassen, T., et al., "Modeling and Simulation of an Electro-Mechanically Actuated Pushbelt Type Continuously Variable Transmission," Mechatronic Systems 2004: A Proceedings Volume From the 3rd IFAC Symposium, Sydney, Australia, Sep. 2004.
22. Togai, K., and Koso, M., "Dynamic Scheduling Control for Engine and Gearshifts: Consolidation of Fuel-Economy

Optimization and Reserve Power," Mitsubishi Motors Technical Review No. 18, 2006.
23. Anthony, J., Moskwa, J., and Danielson, E., "Powertrain Simulation of the M1A1 Abrams Using Modular Model Components," SAE International Congress & Exposition, Detroit, MI, Feb. 1998.
24. Assanis, D., et al., "Validation and Use of SIMULINK Integrated, High Fidelity, Engine-in-Vehicle Simulation of the International Class VI Truck," SAE Transactions, Vol. 109, No. 3, pp. 384–399, 2000.
25. Fathy, H., Ahlawat, R., and Stein, J., "Proper Powertrain Modeling for Engine-in-the-Loop Simulation," Proceedings of the 2005 ASME International Mechanical Engineering Congress and Exposition, Orlando, FL, 2005.
26. Yi, J., Wang, X., Hu, Y., and Li, C., "Fuzzy Control and Simulation on Automatic Transmission of Tracked Vehicle in Complicated Driving Conditions," 2006 IEEE International Conference on Vehicular Electronics and Safety, pp. 259–64, 2007.
27. Nedungadi, A., Pozolo, M., and Mimnagh, M., "A General Purpose Vehicle Powertrain Modeling and Simulation Software-VPSET," 2008 World Automation Congress Conference, Waikoloa, HI, 2008.
28. Bauman, S.W., and Lewicki, D.G., "Refined Gearbox Design for the Chariot Lunar Rover," Proceedings of the 40th Aerospace Mechanisms Symposium, NASA Kennedy Space Center, May 7–9, 2010.
29. Lacraru, L.M. and Bouazza-Marouf, K., "Friction compensation of an actively restrained clutch for path tracking," Proc. of the IMechE, Part I: J. of Sys. and Ctrl. Engr. Vol. 220, No. 5, pp. 381–393, 2006.

REPORT DOCUMENTATION PAGE	Form Approved OMB No. 0704-0188

1. REPORT DATE *(DD-MM-YYYY)*	2. REPORT TYPE	3. DATES COVERED *(From - To)*
01-05-2010	Technical Memorandum	

4. TITLE AND SUBTITLE
Two-Speed Gearbox Dynamic Simulation Predictions and Test Validation

5a. CONTRACT NUMBER

5b. GRANT NUMBER

5c. PROGRAM ELEMENT NUMBER

6. AUTHOR(S)
Lewicki, David, G.; DeSmidt, Hans; Smith, Edward, C.; Bauman, Steven, W.

5d. PROJECT NUMBER

5e. TASK NUMBER

5f. WORK UNIT NUMBER
WBS 877868.02.07.03.01.01.01

7. PERFORMING ORGANIZATION NAME(S) AND ADDRESS(ES)
National Aeronautics and Space Administration
John H. Glenn Research Center at Lewis Field
Cleveland, Ohio 44135-3191

8. PERFORMING ORGANIZATION REPORT NUMBER
E-17299

9. SPONSORING/MONITORING AGENCY NAME(S) AND ADDRESS(ES)
National Aeronautics and Space Administration
Washington, DC 20546-0001

10. SPONSORING/MONITOR'S ACRONYM(S)
NASA

11. SPONSORING/MONITORING REPORT NUMBER
NASA/TM-2010-216363

12. DISTRIBUTION/AVAILABILITY STATEMENT
Unclassified-Unlimited
Subject Category: 37
Available electronically at http://gltrs.grc.nasa.gov
This publication is available from the NASA Center for AeroSpace Information, 443-757-5802

13. SUPPLEMENTARY NOTES

14. ABSTRACT
Dynamic simulations and experimental validation tests were performed on a two-stage, two-speed gearbox as part of the drive system research activities of the NASA Fundamental Aeronautics Subsonics Rotary Wing Project. The gearbox was driven by two electromagnetic motors and had two electromagnetic, multi-disk clutches to control output speed. A dynamic model of the system was created which included a direct current electric motor with proportional-integral-derivative (PID) speed control, a two-speed gearbox with dual electromagnetically actuated clutches, and an eddy current dynamometer. A six degree-of-freedom model of the gearbox accounted for the system torsional dynamics and included gear, clutch, shaft, and load inertias as well as shaft flexibilities and a dry clutch stick-slip friction model. Experimental validation tests were performed on the gearbox in the NASA Glenn gear noise test facility. Gearbox output speed and torque as well as drive motor speed and current were compared to those from the analytical predictions. The experiments correlate very well with the predictions, thus validating the dynamic simulation methodologies.

15. SUBJECT TERMS
Transmissions (machine elements); Gears; Clutches; Rotary wing aircraft; Dynamic models

16. SECURITY CLASSIFICATION OF:			17. LIMITATION OF ABSTRACT	18. NUMBER OF PAGES	19a. NAME OF RESPONSIBLE PERSON
a. REPORT	b. ABSTRACT	c. THIS PAGE			STI Help Desk (email:help@sti.nasa.gov)
U	U	U	UU	19	19b. TELEPHONE NUMBER *(include area code)* 443-757-5802